



Effect of Laser Remelting on the Microstructural and Mechanical Properties of High-Velocity Oxy-Fuel (HVOF)-Sprayed WC-NiCr Coating

Navneet K. Singh¹ · Gidla Vinay² · Harpreet Singh² · Partha Pratim Bandyopadhyay¹

Submitted: 19 December 2023 / in revised form: 23 April 2024 / Accepted: 24 April 2024 / Published online: 21 May 2024
© ASM International 2024

Abstract WC-based coatings are found efficient in providing excellent tribological properties to the structures and components subjected to harsh wear and erosion environments. High-velocity oxy-fuel (HVOF) spraying is known as one of the best techniques to deposit such coatings. However, there still exists scope for further microstructural refinement and improvement in the mechanical properties of the as-sprayed HVOF coatings. Laser remelting has proven to be an appropriate process to achieve such improvement in as-sprayed WC-based coatings. In the current investigation, laser remelting at two different power levels was done on the HVOF-sprayed WC-NiCr coating on stainless steel specimens. The post-processed coatings were analyzed using a scanning electron microscope, x-ray diffraction, x-ray photoelectron spectroscopy, and ImageJ software to study the microstructural changes. Microhardness and surface roughness measurements were also performed to study the mechanical changes. The laser remelting resulted in a smoother coating surface, having lower porosity, lower surface roughness, and higher microhardness as compared to the as-sprayed HVOF coatings. The highest reduction in the porosity was found to be around 72%, whereas, an increment of around 21% in the microhardness was witnessed. These two parameters are crucial for the tribological performance of the coatings.

The current study also gives direction to further study these remelted coatings in tribological conditions.

Keywords laser remelting · *microstructural refinement* · surface modification · thermal spray coatings

Introduction

Thermal spraying is a group of processes that find application across a wide range of industries for developing protective coatings. This technology allows for the utilization of a diverse array of materials, including metals, metal alloys, ceramics, hard metals, composites, and polymers to generate the coatings (Ref 1). Thermal spraying includes various spray methods, including flame spraying, arc spraying, high-velocity flame spraying, plasma spraying, and cold gas dynamic spray processes. Out of the various thermal spraying methods, the high-velocity oxygen fuel (HVOF) spraying has displayed encouraging and promising outcomes. HVOF thermal spray deposition is a surface engineering method extensively employed in industry to enhance the performance of mechanical components, particularly in terms of wear resistance and corrosion resistance (Ref 2-4). Sidhu et al. (Ref 5) conducted a comparative analysis of different thermal spraying methods, and their findings indicated that the HVOF spraying process outperforms other thermal spraying techniques such as flame spraying, plasma spraying, and electric arc spraying in key aspects including flame temperature, porosity, bond strength, and particle velocity. They also determined that HVOF spraying preserves the feedstock powder's chemical composition and mechanical properties of the target surface.

✉ Partha Pratim Bandyopadhyay
ppb@mech.iitkgp.ac.in

¹ Department of Mechanical Engineering, Indian Institute of Technology Kharagpur, Kharagpur, West Bengal 721302, India

² Department of Mechanical Engineering, Indian Institute of Technology Ropar, Rupnagar, Punjab 140001, India

Majorly the applications of thermal spraying concentrate on the tribology of mechanical components that experience relative motion, including pistons, gears, pumps, cylinders, valves, bearings, and braking systems (Ref 6-8). The literature suggests that WC-based HVOF-sprayed coatings are a good alternative for increasing the lifespan of such components (Ref 9-11). The good performance of such coatings in the wear atmosphere is attributed to their robust adhesion, superior cohesive strength, minimal residual stresses, and impressive wear resistance. Bolelli et al. (Ref 12) deposited TiC-FeCrAl by HVOF and evaluated its wear performance against WC-CoCr coating. They found that the wear performance of the former coating was inferior to the WC-CoCr coating due to extensive brittle fracture in the TiC-FeCrAl coating. Houdkova et al. (Ref 13) studied different coating combinations including WC-Hastelloy and NiCrSiB coating. They concluded that all the tested materials exhibited inferior wear resistance when compared to WC-CoCr coating owing to their inferior mechanical properties to WC-CoCr coating.

According to the European CLP directive on the classification and labeling of hazardous substances, metallic cobalt was labeled as a carcinogen material (Ref 14). However, in recent years, nickel-based WC coatings have been considered a potential alternative to cobalt-based WC coatings in the wear and marine environment due to their eco-friendly properties and excellent corrosion resistance (Ref 15-18). Singh et al. compared the wear and corrosion performance of two nickel-based coatings, i.e., WC-10Ni5Cr and WC-18Hastelloy C, and concluded that the former coating outperformed the latter one owing to its superior mechanical and microstructural properties (Ref 19-21).

In general, the particles sprayed by HVOF are initially in a molten state. However, before coming into contact with the surface, not all particles maintain this state upon impact. Consequently, small cavities or micropores are detected within the coating and at the interface of the base material (Ref 22-24). These imperfections, coupled with the absence of a metallurgical bond between the substrate and the coating, impose limitations on the applicability of HVOF, especially in situations demanding higher levels of wear, corrosion, and impact resistance. Murugan et al. (Ref 25) investigated the relationship between the hardness of WC-CoCr coatings and their porosity levels, revealing a decrease in hardness in coatings with greater porosity. Consequently, it becomes evident that this condition diminishes the longevity of certain mechanical components. In this regard, homogenization of the microstructure of HVOF-sprayed coating by reducing the porosity using a laser remelting (LR) process has been proven to be beneficial (Ref 25-31). Laser remelting is a well-established technique for enhancing the surface properties of coatings,

including microstructure, microhardness, and wear resistance (Ref 32-34). In this process, a high-power laser generates a beam that is directed onto the coated surface. The irradiated area forms a molten pool, enabling better metallurgical bonding between substrate and coating (Ref 35, 36). As the laser source moves over the molten pool, the material undergoes a transition from a solid surface to a molten one, leading to the development of residual stresses. Zhang and Kong (Ref 37) have investigated that the generated residual stress due to the laser remelting improved the bonding strength of the as-sprayed coating. The improved properties of the laser-treated coating surface resulted from the distinctive attributes of laser radiation, including its high beam coherence, power versatility, availability, and a broad range of energy density (Ref 38). It has been evident from the literature that laser remelting can be used as an effective method that fosters considerable enhancements in porosity reduction, adhesion, and tribological properties of HVOF-sprayed coatings (Ref 39-43). It can be concluded from the above discussion that laser remelting can enhance the microstructural and mechanical properties of HVOF-sprayed coatings.

In our previous studies, we have established that HVOF-sprayed WC-NiCr coatings are a good alternative as a protective coating against wear (Ref 19-21). To further improve the wear resistance of this coating, reducing the porosity using post-processing techniques is considered to be useful. It has been proven that the laser remelting of HVOF-sprayed WC-CoCr coating would produce remelting and densification within the coating, producing a microstructure with a much lower porosity (Ref 44). As per the observation of this study, it was anticipated that the same effect of laser remelting could be observed for a similar coating combination (WC-NiCr). According to the literature cited in the previous sections, a decrease in porosity could lead to an increase in the microhardness of the as-sprayed coatings (Ref 45, 46). However, to the knowledge of the authors, laser remelting has not been employed as a post-processing technique for HVOF-sprayed WC-NiCr coating. In this context, our research is focused on using laser remelting on the HVOF-sprayed WC-NiCr coating at two power levels; 300 and 500 W, to refine the microstructure of the coating, study the phase changes during the remelting, reducing the porosity, and increasing the microhardness within the HVOF-sprayed WC-NiCr coating. The primary objective of this study is to establish the viability of the laser remelting process in the post-processing of the HVOF-sprayed WC-NiCr coating to achieve the desired changes in the microstructural and mechanical properties of the investigated coating. The outcome of this research will give a direction to utilize laser remelting of HVOF-sprayed WC-NiCr coating to generate a better wear-resistant coating than the as-sprayed coating.

Materials and Methods

Materials and Deposition Process

In the present study, the substrate material (18Cr-8Ni austenitic stainless steel) was provided by Passi Machine Tools, Ludhiana, India. The substrates were sliced into coupons of size 20 mm * 20 mm * 5 mm using electric discharge machining (EDM) (ELECTRONICA, SPRINT-CUT, India). The feedstock powder, WC-10Ni5Cr (WOKA 3552), was procured from Oerlikon Metco AG (Wohlen, Switzerland). For convenience, the feedstock powder is named as WC-NiCr hereafter. These commercially available agglomerated and sintered powders had a particle size distribution of $-45 + 15 \mu\text{m}$. The feedstock powder was characterized using a scanning electron microscope: SEM (JEOL, JSM-6610LV, Japan) and electron-dispersive x-ray spectroscopy (EDS) with regard to the powder morphology, elemental analysis, and average particle size.

Elemental analysis of the steel substrate was done by stationary optical emission spectrometers (OES) using Foundry Master Smart, Hitachi, UK. Positive material identification technique was adopted to obtain the elemental information of feedstock material at the Institute for Auto Parts and Hand Tools Technology Ludhiana, Punjab, India. The results of the elemental analysis are given in Table 1a and b.

The degreased and preheated substrates were grit blasted with Virgin Brown aluminum oxide (Al_2O_3) particles of grit size 16 with an operating pressure of 4 kg/cm^2 to eliminate impurities and to provide adequate surface roughness required for strong bonding at the coating–substrate interface. Grit blasting was done at M/S Metallizing Company Private Limited, Jodhpur (India), using a pressure blasting machine (MEC, PB-1982, India). The prepared substrates were then coated with WC-NiCr powder using HVOF spraying equipment (MECPL, HIPOJET-2700, India). The parameter selection for this work has

been taken from a previous work done by Goyal et al. (Ref 47). The deposition parameters are presented in Table 2.

Laser Remelting Technique

The schematic of the laser remelting technique used for this study is shown in Fig. 1. The HVOF-sprayed coating was post-treated using a fiber laser source (Raycus, China) having a wavelength of 1080 nm. Laser remelting was done using two distinct power (300 and 500 W). The coatings treated with 300 W were named LM1, whereas the coatings treated with 500 W were named LM2. The scanning speed and laser spot diameter were kept at 2000 mm/min and 3 mm, respectively. The laser remelting was done in a protective argon environment to limit the oxidation of the as-sprayed coatings.

Microstructural and Mechanical Characterization

The feedstock powder was characterized using a scanning electron microscope (JEOL, JSM-6610LV, Japan) to study the powder morphology. ASTM E1920 (Ref 48) guide was followed to prepare the coated samples for further

Table 2 HVOF operating parameters adopted to coat WC-NiCr coating on 18Cr-8Ni stainless steel

HVOF spraying operating parameter	Value
Oxygen flow rate, slpm	250-270
Oxygen pressure, kg/cm^2	10
Fuel (LPG) flow rate, slpm	55-65
Fuel pressure, kg/cm^2	6.5
Air flow rate, slpm	700-750
Air pressure, kg/cm^2	6.5
Spray velocity, m/s	450
Powder feed rate, g/min	40

Table 1 Elemental analysis of (a) steel substrate and (b) feedstock powder used

Material	Chemical composition, wt.%							
	C	Si	Mn	P	Cr	S	Mo	Ni
18Cr-8Ni SS	0.045	0.46	1.40	0.041	18.0	0.013	0.227	8.31

Material	Chemical compositions, wt.%					
	WC	Ni	Cr	Fe	Co	Mn
WC-NiCr	Rest	10.59	5.85	0.13	0.14	0.01

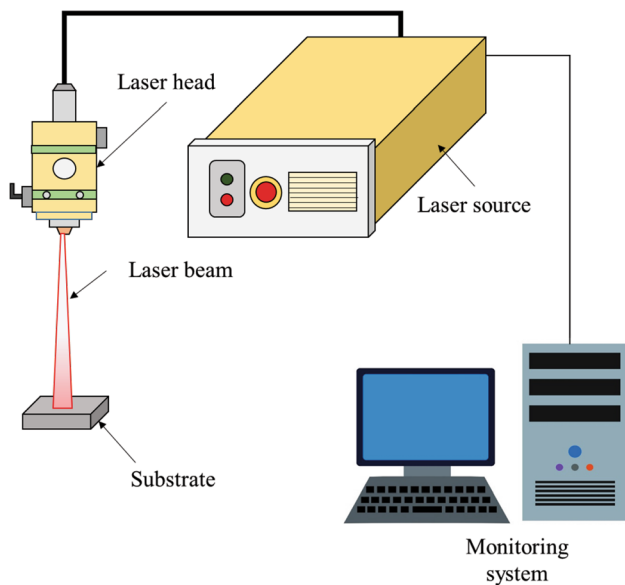


Fig. 1 Laser remelting schematic used for post-processing of HVOF-sprayed WC-NiCr coating

metallurgical studies. SEM was used to visualize the microstructural information of as-sprayed and laser-remelted coatings. The coating–substrate interface was also studied under SEM to visualize the bonding of the coating material to the substrate. This was done by sectioning the coating–substrate assembly. The analysis of magnified (1000x) secondary electron SEM images from five different locations was done using ImageJ software to determine the porosity in the as-sprayed and laser-remelted coatings.

X-ray diffraction (XRD) of the unpolished as-sprayed and laser-remelted coatings was conducted using Analytical X-pert Pro, Netherlands. XRD was used to analyze the phases present in the as-sprayed coating and to identify any observable phase alterations that occurred during the laser remelting process. The remelting caused by the application of a high-energy laser may result in the formation of new phases in the coating. The exposure of the material to the atmosphere may also result in the formation of oxides. The XRD peaks were matched using X-pert High Score software (Malvern Panalytical). To understand the phase changes that occurred in the coatings during laser remelting, x-ray photoelectron spectroscopy (XPS) was done on the polished surface of the investigated materials, i.e., as-sprayed, LM1, and LM2. The XPS analysis was performed using Escalab 250Xi (Thermo Fisher Scientific) available at Central Research Facility, IIT Ropar. XPS survey spectrum was carried out on all the coatings to understand the binding energy range of the selected core elements. An x-ray ($Al K\alpha$) with a spot size of $650 \mu m$ and step size of 1 eV and 0.1 eV is used for obtaining survey scan and core elements, respectively.

Charge compensation was applied for all the measurements, and the charge correction was done by taking carbon (C1s) as a reference. The peak fitting for the core elements was performed by using commercially available Thermo Advantage software, and graphs are plotted using Origin 8.0.

Microhardness indentation testing was conducted on both the coatings and the substrate using an instrumented indenter (WILSON 402MVD, China). This indenter was equipped with a Vickers indenter, and the testing procedure adhered to the standards outlined in ASTM C 1327 (Ref 49). The load and dwell time in this measurement were kept at 300 g and 10 s, respectively. A minimum of 10 indents were made across the transverse section of the as-sprayed and laser-remelted coatings, and the resultant average values were reported.

The average surface roughness (R_a) was measured using a profilometer equipped with a $2\text{-}\mu m$ tip radius (ZEISS, SURFCOM 130 A, Japan). A total of twelve measurements were conducted for each sample, and the resultant average values were reported.

Results and Discussion

Microstructural Characterization of Feedstock Powder and Developed As-Sprayed Coating

SEM analysis was done to reveal the WC-NiCr powder morphology. The feedstock powder displayed an almost spherical shape with surface irregularities forming a sponge-like texture as shown in Fig. 2(a). The particle size of the feedstock was found to be in the range quoted by the supplier. The cross-sectional image of the feedstock is depicted in Fig. 2(b). Elemental composition and mapping was done on the cross-section of the feedstock, and the results are shown in Fig. 2(c), (d), (e), (f), (g), and (h). The elemental composition was found to be similar as discovered through the positive material identification technique as shown in Table 1b. The EDS mapping shows a uniform distribution of each element in the feedstock powder.

The cross-sectional SEM image of WC-NiCr-coated steel is presented in Fig. 3(a). The thickness of the deposited coating was found in the range of $250 \pm 20 \mu m$. The image reveals a well-defined interface between the substrate and the as-sprayed coating, exhibiting continuous interfacial contact. This observation suggests a strong bond (as depicted in Fig. 3b) between the substrate and the coating.

The enlarged view of the as-sprayed WC-NiCr coating is illustrated in Fig. 3(c). The SEM image of WC-NiCr coating consists of both the carbide (WC) and binder (NiCr) phases. The developed coating surface depicts a

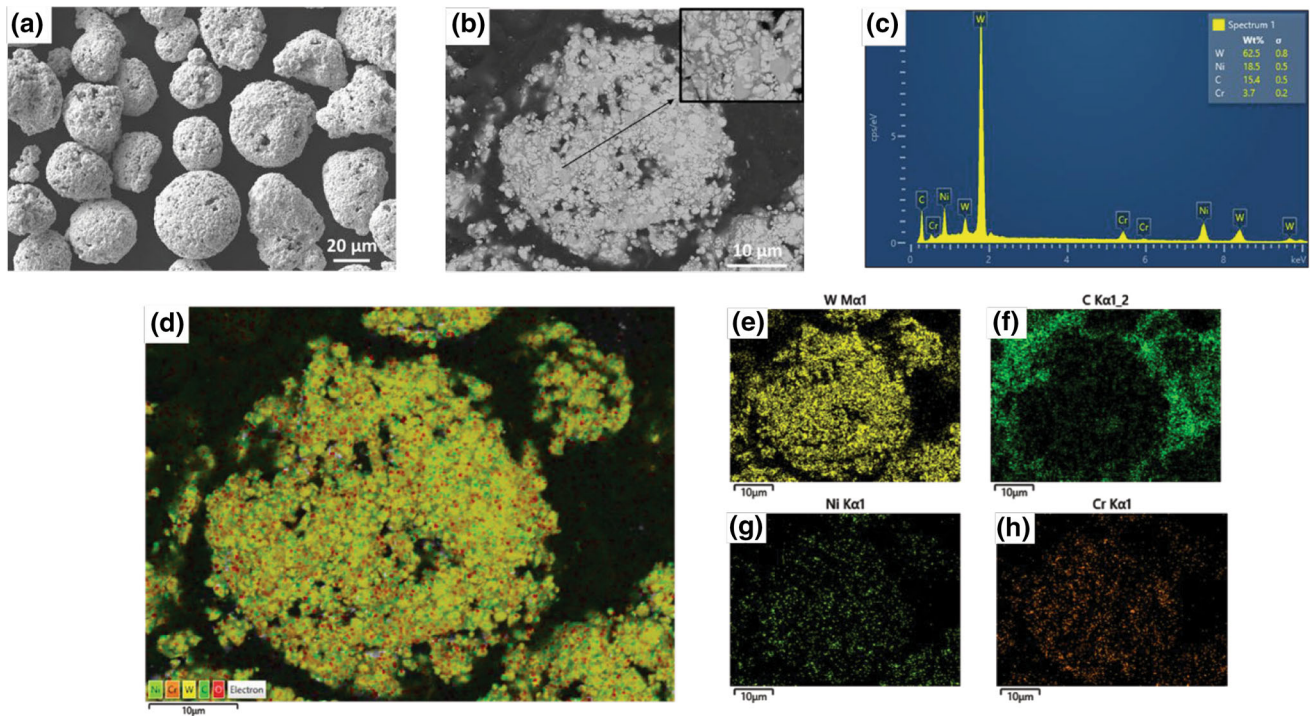


Fig. 2 (a) SEM micrograph, (b) cross-sectional SEM micrograph, (c) elemental distribution, and (d–h) elemental mapping of WC-NiCr powder

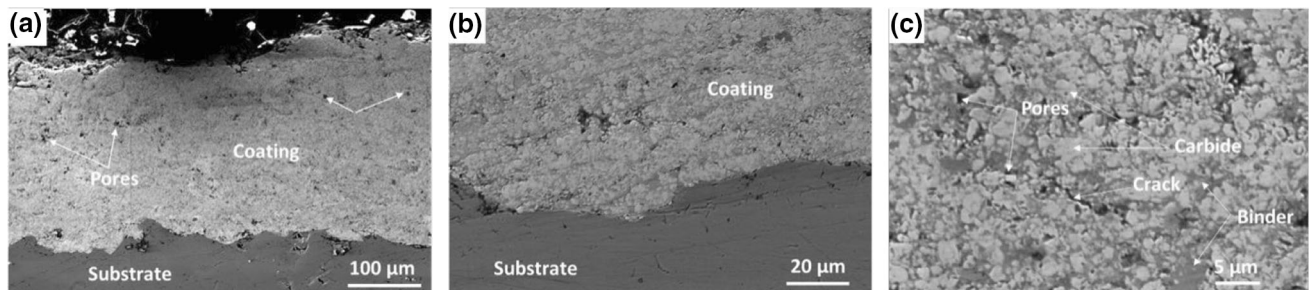


Fig. 3 Secondary electron image showing (a) cross-section of the coating–substrate interface, (b) enlarged view of the cross-section, and (c) enlarged view of the HVOF-sprayed WC-NiCr coating

well-bonded and dense structure owing to the nice retention of WC particles within the NiCr matrix. However, there is evidence of some micropores and cracks on the surface of the coating. The dissimilar melting temperatures of WC and the binder led to a scenario in which WC particles remained partially molten, surrounded by metal binders. The difference between the carbide and binder phases is identified in the micrograph. Fine angular carbide particles appeared light gray and were encased by dark gray binder phase. As shown in Fig. 3(b), it is evident that WC particles are neatly arranged within the binder, accompanied by a few micropores. This arrangement enhances the coating's compactness and promotes robust interlamellar cohesion. Before applying the coating, the surface roughness of the steel substrate was enhanced

through grit blasting. The surface roughness of the steel increased to $7.8 \pm 0.02 \mu\text{m}$ after the grit blasting. This increased surface roughness plays a crucial role in facilitating effective mechanical bonding between the substrate and the coating material. A similar finding was reported by Gonzalez-Hermosilla et al. (Ref 50), highlighting that the enhanced surface roughness resulting from grit blasting leads to improved mechanical bonding between the substrate and the coating.

Effect of Laser Remelting on the As-Sprayed Coating

The comparison of the surface morphology of as-sprayed and laser-remelted WC-NiCr coatings is shown in Fig. 4.

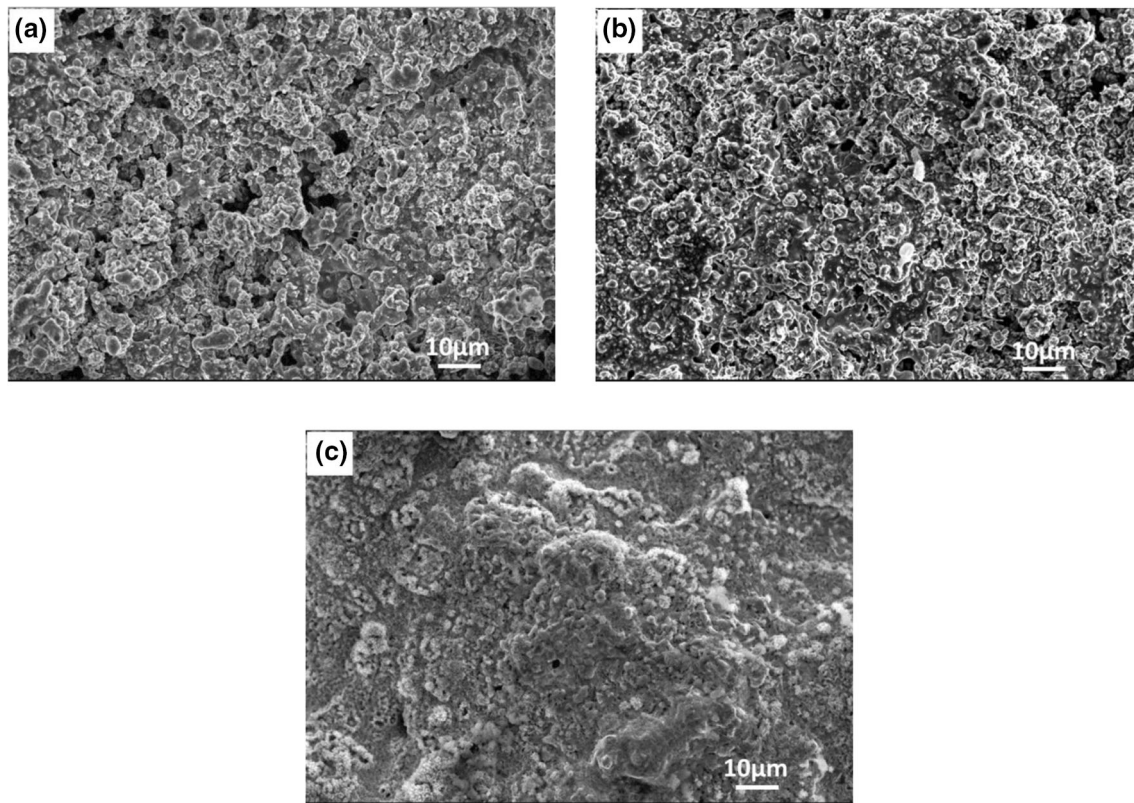


Fig. 4 Secondary electron images showing the surface morphology of (a) as-sprayed WC-NiCr coating, (b) laser-remelted (300 W) WC-NiCr coating (LM1), and (c) laser-remelted (500 W) WC-NiCr coating (LM2)

The surface of laser-remelted coatings appears to be tightly packed in contrast with the untreated coating depicted in Fig. 4(a).

In general, there exist partially melted WC particles in as-sprayed HVOF coatings, as discussed above. Under the application of laser remelting, these particles undergo a further degree of melting, followed by solidification, causing better compacting and encasing of these WC particles in the binder matrix. For the same reason, the LM1 and LM2 surfaces seem more compact when compared to the as-sprayed coating surface. However, due to a higher degree of remelting caused using laser remelting at 500 W, the LM2 coating surface appears to be more refined and compact when compared to the LM1 surface.

The surface roughness studies of the investigated coatings also support the above claim. The average surface roughness values for the investigated coatings are presented in Table 3. It can be analyzed that, in general, laser remelting reduced the roughness level of the as-sprayed coatings. A reduction of nearly 9% and 12% has been observed in LM1 and LM2 coatings, respectively, when compared to the surface roughness of as-sprayed coatings. The cross-sectional coating–substrate interface and the morphology of all the developed coatings are presented in Fig. 5.

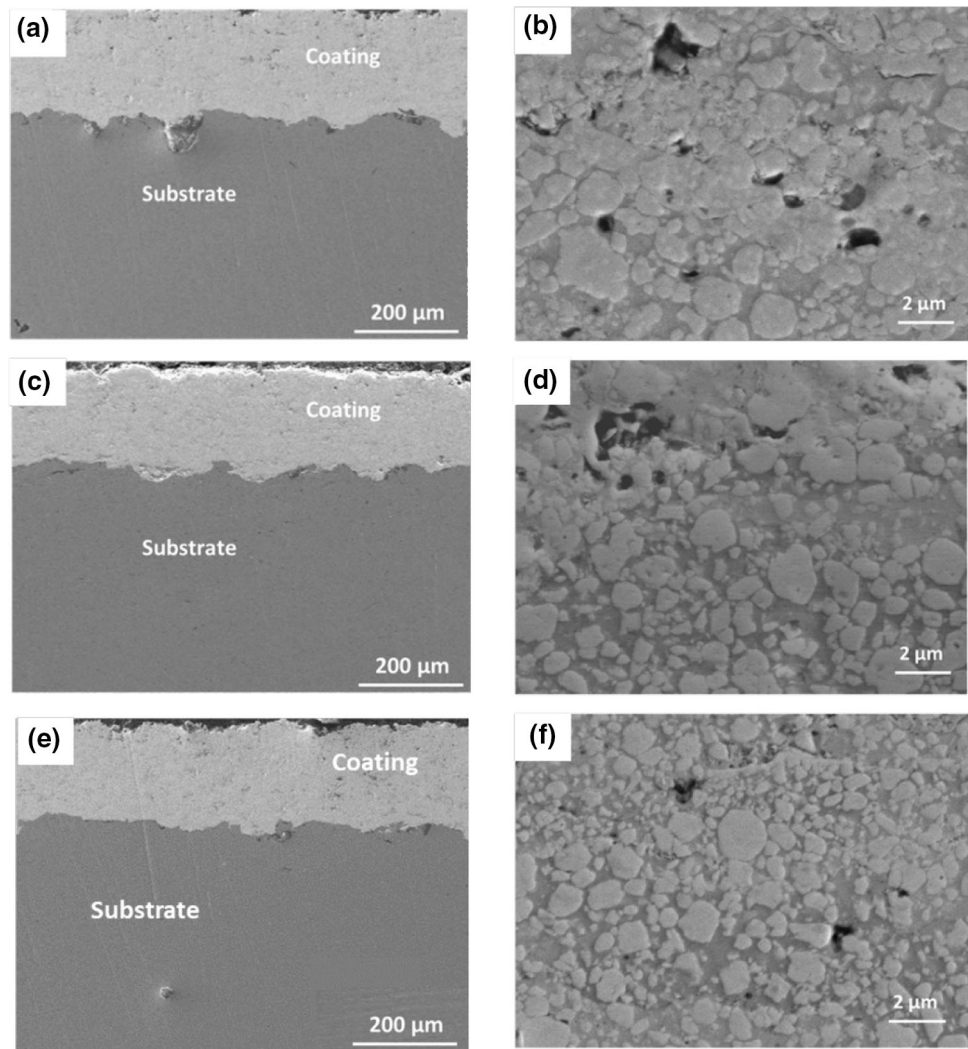
Table 3 Average porosity and average surface roughness of as-sprayed and laser-remelted WC-NiCr coatings

Material	Porosity, %	Surface roughness, μm
As-sprayed WC-NiCr	2.2 ± 0.6	1.9 ± 0.1
LM1	1.6 ± 0.3	1.7 ± 0.1
LM2	0.6 ± 0.2	1.6 ± 0.1

In all the cases, a clear interface can be seen between the coatings and their respective substrate indicating that the coatings are still well adhered to the substrate after the post-processing as shown in Fig. 4(a), (b), and (c). However, the visibility of pores was reduced in laser-remelted coatings when compared to the visible pores in the as-sprayed coating, depicted in the enlarged view of the coatings as shown in Fig. 4(b), (d), and (f).

To support the above claim, quantification of these pores was done using ImageJ software. The average porosity values of the investigated coatings are tabulated in Table 3. It can be noticed that the maximum porosity was present in as-sprayed HVOF coating, and the porosity was further reduced in LM1 followed by LM2 coating. The quantitative comparison depicts that the porosity value in LM1 is

Fig. 5 Secondary electron images showing the coating–substrate interface and coating morphology of (a, b) as-sprayed WC–NiCr coating, (c, d) laser-remelted (300 W) WC–NiCr coating (LM1), and (e, f) laser-remelted (500 W) WC–NiCr coating (LM2)



nearly 30% less than in as-sprayed coating. However, in comparison with as-sprayed coating, a porosity reduction of about 72% was observed in the case of LM2. This is attributed to the high energy associated with operating the laser at 500 W. Significant modification in the microstructure of the coating was observed on the LM2 surface due to the higher degree of remelting compared to that of the LM1 coating operated at 300 W. This observation affected the visibility of pores in both the laser-remelted coatings. A similar observation was reported by Castro et al. (Ref 44) while remelting the HVOF-sprayed WC–CoCr coating at 400 and 600 W.

XRD peaks obtained for as-sprayed, LM1, and LM2 coatings are shown in Fig. 6. It shows that the HVOF-sprayed WC–NiCr coatings, obtained using the process parameters listed in Table 2, are successful in depositing coatings with low oxide content.

In the as-sprayed coating, the presence of WC and NiO phases is observed alongside the detection of W_2C peaks.

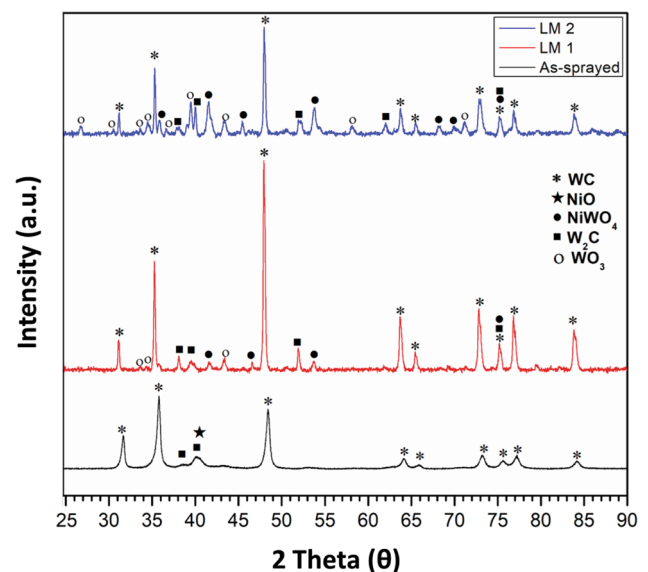


Fig. 6 X-ray diffractions of as-sprayed HVOF coating, laser-remelted coating (LM1), and laser-remelted coating (LM2)

During the HVOF spraying process, the carbide within the WC undergoes decarburization, transforming into W_2C due to the high temperatures involved. This phenomenon of WC decarburization into W_2C is commonly observed in HVOF-sprayed WC-based coatings. The lower levels of decarburization are generally referred to as WC and exhibit greater stability and improved properties in their original state. In the present coating, a low level of decarburization is observed during the coating formation, which is favorable for its performance in the as-coated condition. Upon laser remelting of the as-sprayed coatings, LM1, and LM2, the appearance of new peaks is evident, corresponding to phases such as W_2C , WO_3 , and $NiWO_4$. As previously mentioned, WC undergoes decarburization to form W_2C initially. Subsequent exposure to heat and interaction with the surrounding atmosphere leads to its further conversion into the WO_3 state. A study was done by Chen et al. (Ref 51), to understand the oxidation mechanism in WC-CoCr composites. They observed that WC starts oxidizing at around 450 °C where WC changes to WO_3 . They also observed that part of W also reacted with Co and formed compounds like $CoWO_4$, which here can be related to the formation of $NiWO_4$. In the current investigation, among the laser-treated samples, LM2 undergoes greater temperature elevation due to the application of higher laser energy. This results in an overall increase in the temperature, thereby enhancing the likelihood of WO_3 formation. A comparison of the XRD patterns between LM2 and LM1 reveals a more prominent presence of WO_3 and $NiWO_4$ in LM2 compared to LM1. This increase is purely attributable to the higher temperatures translated from the usage of high laser power.

Information on the chemical state of the elements present in the coatings has been investigated by XPS. A simple survey spectrum which means obtaining binding energy data of the specimen over the complete range reveals the presence of the prominent elements. Figure 7(a), (b), and (c) shows the survey spectrum results of the as-sprayed coating, LM1, and LM2, respectively. Survey spectrum results confirm the presence of W, C, O, Ni, and Cr in the coating. It is observed that Oxygen content has increased for LM1 and LM2 when compared with the as-sprayed while W content has decreased.

XPS of core elements W and Ni scan is shown in Fig. 7(d), (e), (f), (g), (h), and (i). For as-sprayed coating, it can be observed that W exhibits three peaks at 31.7, 33.8, and 36.3 eV (Fig. 7d). The initial two peaks represent W 4f 7/2 and W 4f 5/2 peaks of W. This is a W^{2+} state of W when bound with WC. The later peak represents W 5p3/2 of WC (Ref 51). This confirms that most of the WC is retained in the carbide phase with minimal decarburization or oxide formation of WC during the coating generation. For LM1 (Fig. 7e), additionally, two more peaks are

observed for the W elements at 35.5 and 37.7. These two peaks correspond to the W 4f 7/2 and W 4f 5/2 peaks of W^{6+} from WO_3 which confirms the oxidation of the W (Ref 34). The results are consistent with the previous studies on the oxidation of WC (Ref 52–55). For LM2 (Fig. 7f), the WO_3 peaks at binding energies 35.5 eV and 37.7 eV have increased further by decreasing the WC percentage which confirms the XRD results. This observation confirms our previous claim that due to the higher laser power, temperature has significantly increased which played an important role in phase formation.

Figure 7(g), (h), and (i) shows the XPS results of Ni 2p for as-coated, LM1, and LM2, respectively. The two dominant peaks at binding energies 855.9 eV and 873.8 eV correspond to the Ni 2p3/2 and Ni 2p1/2 spin orbit while the remaining two are identified as shake-up satellite peaks (Ref 56). These features reveal that Ni is in the form of a + 2 oxidation state which confirms the oxidation of Ni (Ref 57). In the as-sprayed state, Ni is exhibiting the binding energy of 853.1 eV which corresponds to the NiO state while the binding energies of 855.9 eV and 856 eV observed in the LM1 and LM2 samples, respectively, correspond to the Ni binding energy in the $NiWO_4$ state (Ref 57). This complements the findings of the XRD. Figure 7(j), (k), and (l) shows the XPS results of Cr for as-sprayed, LM1, and LM2, respectively. In as-sprayed state, the Cr is exhibiting two peaks at binding energies 574.3 eV and 576.5 eV. The former corresponds to the Cr in metal state while the latter corresponds to the Cr (III) type oxide. It is observed that Cr remains in metal form in the coating. However, with the laser remelting, Cr is completely changed into its oxide state which is observed at binding energy 576.3 eV for LM1 and LM2. The oxide state of the Ni and Cr in as-sprayed state could be attributed to the high temperature involved during the coating generation using HVOF.

Microhardness of the Developed Coatings

The average microhardness was measured with a load of 300 g. The microhardness of the as-sprayed WC-NiCr coating was found around 1102 ± 96 HV. Upon laser remelting, the enhancement in the microhardness of the as-sprayed coating was witnessed. For LM1, the average microhardness was found around 1222 ± 76 HV. Whereas, in the case of LM2, the average microhardness was found around 1332 ± 78 HV. The variation of microhardness values in the investigated coatings is shown in Fig. 8(a). An increase of around 11% in the microhardness was observed in LM1 when compared to the as-sprayed coating. However, an increase of around 21% in microhardness was witnessed in LM2 coating when compared to as-sprayed coating. One of the main reasons behind this observation is

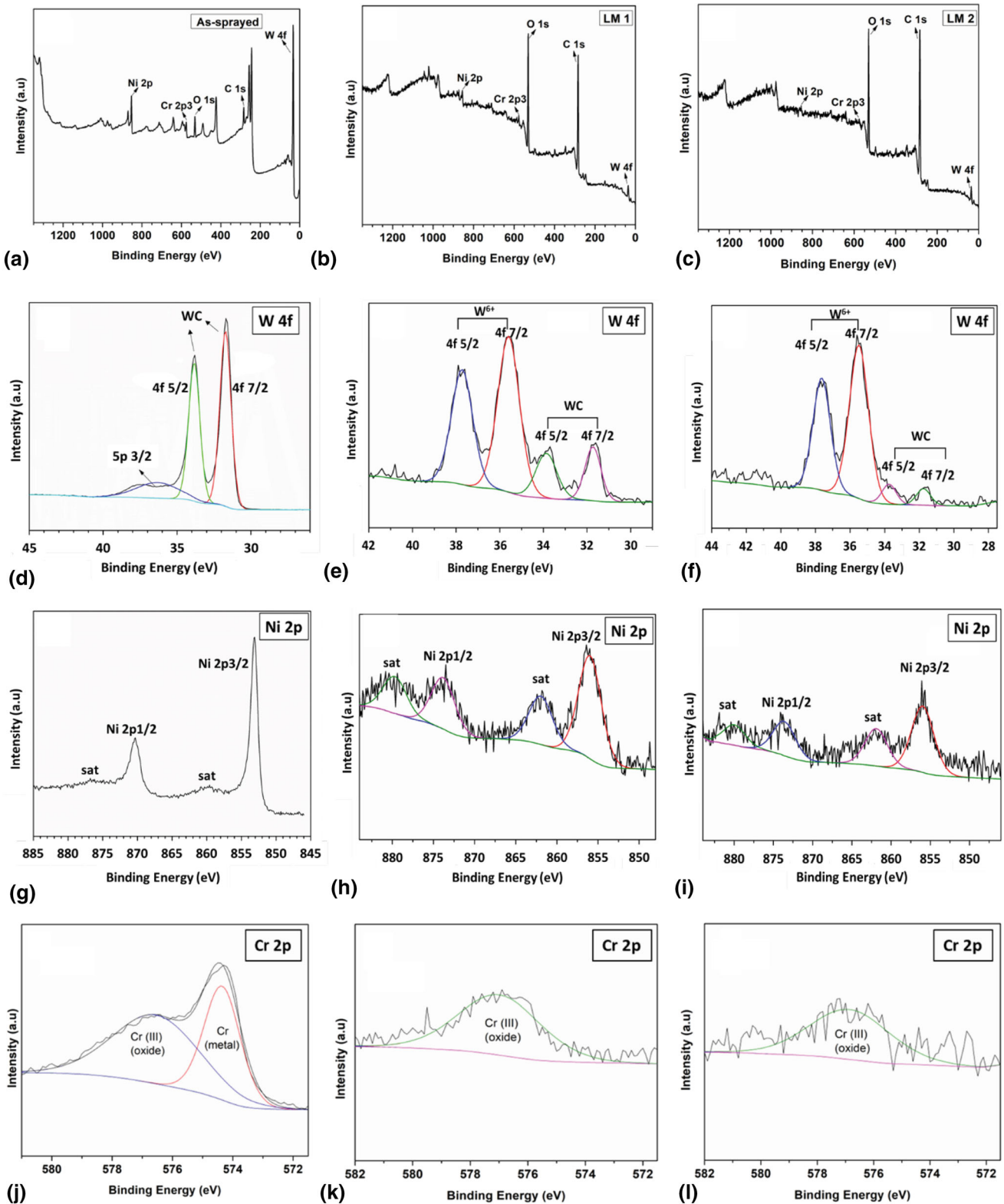


Fig. 7 XPS plots of HVOF-sprayed WC-NiCr coatings showing; survey spectrum scan results of (a) as-sprayed coating, (b) laser-remelted coating, LM1, (c) laser-remelted coating, LM2; W core element scan results for (d) as-sprayed coating, (e) laser-remelted coating, LM1, (f) laser-remelted coating, LM2; Ni core element scan

results for (g) as-sprayed coatings, (h) laser-remelted coatings, LM1, (i) laser-remelted coating, LM2; Cr core element scan results for (j) as-sprayed coatings, (k) laser-remelted coatings, LM1, and (l) laser-remelted coating, LM2

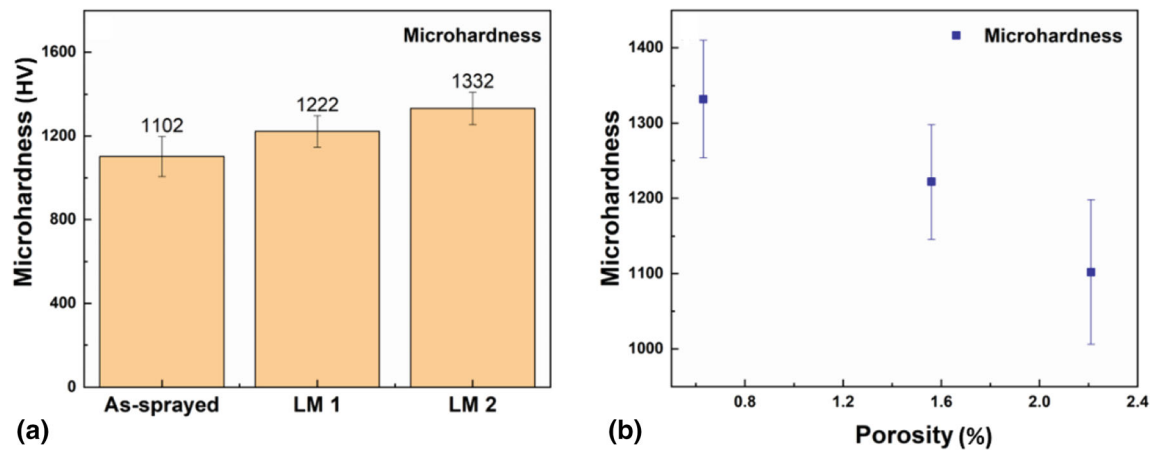


Fig. 8 (a) Average microhardness value of as-sprayed HVOF coating, laser-remelted coating (LM1), and laser-remelted coating (LM2) and (b) relationship of microhardness of the investigated coatings to their respective porosity

the enhanced densification in the laser-remelted coatings. As discussed earlier, LR resulted in lesser porosity in the investigated coatings. The correlation between the porosity and the microhardness of the investigated coatings is shown in Fig. 8(b).

Karthikeyan et al. established an inverse correlation between the porosity and the microhardness of thermal-sprayed coatings (Ref 45). In the present study, Fig. 8(b) shows that the highest hardness was observed in the coating having the lowest porosity and the minimum hardness in the coating having the highest porosity. A similar observation has been reported by Thirumalai Kumarasamy et al., where they concluded that lowering of porosity of a thermal-sprayed coating resulted in enhancement of the microhardness of the coating (Ref 46). These observations indicated that the enhanced microhardness of the LR coatings can be attributed to the decrease in the porosity of the LR coatings.

The improved hardness in the LM1 coating is also attributed to the formation of secondary phases within the coating. Due to this, the precipitation of the WC phase in the binder improved. The better precipitation that occurred was attributed to the difference in the cohesive energies of the WC phase and the mixed secondary phases. The literature suggests that the cohesive energy of the WC phase is 10.64 eV/atom, which is higher than the cohesive energy of secondary formed phases (i.e., WO_3) (Ref 58, 59). For the same reason, these secondary phases got well precipitated in the NiCr matrix (Ref 44). The hardness of the WC phase was also observed as lower when compared to the secondary phases. The above reasonings were responsible for the higher hardness in LM1 when compared to the as-sprayed WC-NiCr coating. Coming to the LM2 coating, the formation of these secondary phases was observed as higher than that of in LM1 coating making it even harder than the LM1 coating. Summarizing the discussions on the

effect of decreased porosity and the secondary formed phases during the laser remelting of the as-sprayed WC-NiCr coating, it can be concluded that the formation of secondary phases along with a decrease in porosity and increase in bonding might have helped in increasing the hardness of the as-sprayed WC-NiCr coating upon laser remelting.

Conclusions

The current study aimed to understand the effect of laser remelting on the microstructural and mechanical properties of the HVOF-sprayed WC-NiCr coating. Two distinct power values (300 and 500 W) were adopted for the remelting. Based on the detailed discussion, the following conclusions have been made:

- The laser remelting technique adopted for the post-processing of HVOF-sprayed WC-NiCr coating progressively produced an increase in the densification of coatings from LM1 to LM2.
- HVOF-sprayed WC-NiCr coating showed an average porosity of 2.21. This porosity decreased by 30% for LM1 and 72% for LM2 upon laser remelting.
- The laser remelting technique adopted for the post-processing of HVOF-sprayed WC-NiCr coating increased the microhardness by 11% for LM1 and 21% for LM2
- The enhanced microhardness of the HVOF-sprayed WC-NiCr coating was attributed to the cumulative effect of the decreased porosity and the formation of secondary phases such as WO_3 , NiWO_4 , and W_2C during the laser remelting
- Laser remelting enhanced the properties of the as-sprayed WC-NiCr coating in terms of densification in

the microstructure of the developed coating with reduced porosity level and increased microhardness. This is attributed to improved melting at a higher power level.

Acknowledgment The authors would like to thank the Science and Engineering Research Board (SERB), Department of Science & Technology (DST), Govt. of India, for providing the fellowship for carrying out this research work under the NPDF scheme (Reference Number: PDF/2022/002265).

References

- H. Koivuluoto, E. Hartikainen, and H. Niemelä-Anttonen, Thermally Sprayed Coatings: Novel Surface Engineering Strategy Towards Icephobic Solutions, *Materials (Basel)*, 2020, **13**, p 1434.
- X.-D. Ding, X. Cheng, C. Li, X. Yu, Z.-X. Ding, and C.-Q. Yuan, Microstructure and Performance of Multi-dimensional WC-CoCr Coating Sprayed by HVOF, *Int. J. Adv. Manuf. Technol.*, 2018, **96**, p 1625-1633.
- X.-T. Luo, G.M. Smith, Y. Wang, E. Gildersleeve, S. Sampath, and C.-J. Li, Cracking Induced Tribological Behavior Changes for the HVOF WC-12Co Cermet Coatings, *Ceram. Int.*, 2018, **45**, p 4718-4728.
- V. Bolleddu, V. Racherla, and P.P. Bandyopadhyay, Comparative Study of Air Plasma Sprayed and High Velocity Oxy-Fuel Sprayed Nanostructured WC-17wt%Co Coatings, *Int. J. Adv. Manuf. Technol.*, 2016, **84**, p 1601-1613.
- T.S. Sidhu, S. Prakash, and R.D. Agrawal, State of the Art of HVOF Coating Investigations—A Review, *Mar. Technol. Soc. J.*, 2005, **39**, p 53-64.
- S.M. Nahvi and M. Jafari, Microstructural and Mechanical Properties of Advanced HVOF-Sprayed WC-Based Cermet Coatings, *Surf. Coat. Technol.*, 2016, **286**, p 95-102.
- G. Ghosh, A. Sidpara, and P.P. Bandyopadhyay, Understanding the Role of Surface Roughness on the Tribological Performance and Corrosion Resistance of WC-Co Coating, *Surf. Coat. Technol.*, 2019, **378**, p 125080.
- F. Ghadami and A. Sabour Rouh Aghdam, Improvement of High Velocity Oxy-Fuel Spray Coatings by Thermal Post-Treatments: A Critical Review, *Thin Solid Films*, 2019, **678**, p 42-52.
- B.S. Mann and V. Arya, Abrasive and Erosive Wear Characteristics of Plasma Nitriding and HVOF Coatings: Their Application in Hydro Turbines, *Wear*, 2001, **249**, p 354-360.
- A.K. Maiti, N. Mukhopadhyay, and R. Raman, Effect of Adding WC Powder to the Feedstock of WC-Co-Cr Based HVOF Coating and Its Impact on Erosion and Abrasion Resistance, *Surf. Coat. Technol.*, 2007, **201**, p 7781-7788.
- V. Kumar, N.K. Singh, R. Verma, D.K. Mahajan, and V.S. Sharma, Corrosion Behaviour of Laser Textured and WCCoCr+GNPs Coated IS-2062 Steel, *Diam. Relat. Mater.*, 2023, **136**, p 109958.
- G. Bolelli, A. Colella, L. Lusvardi, P. Puddu, R. Rigon, P. Sassatelli, and V. Testa, Properties of HVOF-Sprayed TiC-FeCrAl Coatings, *Wear*, 2019, **418-419**, p 36-51.
- Š Houdková, F. Zahálka, M. Kašparová, and L.M. Berger, Comparative Study of Thermally Sprayed Coatings Under Different Types of Wear Conditions for Hard Chromium Replacement, *Tribol. Lett.*, 2011, **43**, p 139-154.
- Commission, E. Commission Delegated Regulation (EU) 2020/217. *Off. J. Eur. Union*, 2020.
- R. Piola, A.S.M. Ang, M. Leigh, and S.A. Wade, A Comparison of the Antifouling Performance of Air Plasma Spray (APS) Ceramic and High Velocity Oxygen Fuel (HVOF) Coatings for Use in Marine Hydraulic Applications, *Biofouling*, 2018, **34**, p 479-491.
- A.S.M. Ang, H. Howse, S.A. Wade, and C.C. Berndt, Manufacturing of Nickel Based Cermet Coatings by the HVOF Process, *Surf. Eng.*, 2016, **32**, p 713-724.
- C.-H. Zhang, C.-L. Wu, S. Zhang, Y.-F. Jia, M. Guan, J.-Z. Tan, and B. Lin, Laser Cladding of NiCrSiB on Monel 400 to Enhance Cavitation Erosion and Corrosion Resistance, *Rare Met.*, 2016, **41**, p 1-9.
- S. Zhang, S. Wu, W. Cui, S. He, C. Zhang, and M. Guan, Cavitation Erosion Properties of Ni-Based RE Alloy Coating on Monel Alloy by Laser Cladding, *Xiyou Jinshu Cailiao Yu Gongcheng/Rare Metals Mater. Eng.*, 2018, **47**, p 1517-1522.
- N.K. Singh, A.S.M. Ang, D.K. Mahajan, and H. Singh, Cavitation Erosion Resistant Nickel-Based Cermet Coatings for Monel K-500, *Tribol. Int.*, 2021, **159**, p 106954.
- N.K. Singh, A. Kumar, A.S.M. Ang, D.K. Mahajan, and H. Singh, Characterization and Slurry Erosion Mechanisms of Nickel-Based Cermet Coatings on Monel K-500, *J. Therm. Spray Technol.*, 2021, **30**, p 2138-2154.
- N.K. Singh, G. Vinay, A.S.M. Ang, D.K. Mahajan, and H. Singh, Cavitation Erosion Mechanisms of HVOF-Sprayed Ni-Based Cermet Coatings in 3.5% NaCl Environment, *Surf. Coat. Technol.*, 2022, **434**, p 128194.
- X. Ding, X.-D. Cheng, X. Yu, C. Li, C.-Q. Yuan, and Z.-X. Ding, Structure and Cavitation Erosion Behavior of HVOF Sprayed Multi-dimensional WC-10Co4Cr Coating, *Trans. Nonferrous Metals Soc. China*, 2018, **28**, p 487-494.
- D. Poirier, J.-G. Legoux, and R. Lima, Engineering HVOF-Sprayed Cr3C2-NiCr Coatings: The Effect of Particle Morphology and Spraying Parameters on the Microstructure, Properties, and High Temperature Wear Performance, *J. Therm. Spray Technol.*, 2013, **22**, p 280-289.
- P.C. Du, X.P. Zhu, Y. Meng, H. Fenq, Q.F. Wong, and M.K. Lei, Water-Lubricated Tribological Behavior of WC-Ni Coatings Deposited by Off-Angle HVOF Spraying, *Surf. Coat. Technol.*, 2017, **309**, p 663-670.
- K. Murugan, A. Ragupathy, V. Balasubramanian, and K. Sridhar, Optimizing HVOF Spray Process Parameters to Attain Minimum Porosity and Maximum Hardness in WC-10Co-4Cr Coatings, *Surf. Coat. Technol.*, 2014, **247**, p 90-102.
- C.R. Ciubotariu, D. Frunzaverde, G. Merginean, V.A. Serban, and A.V. Birdeanu, Optimization of the Laser Remelting Process for HVOF-Sprayed Stellite 6 Wear Resistant Coatings, *Opt. Laser Technol.*, 2016, **77**, p 98-103.
- J. Dutta Majumdar and I. Manna, Laser Material Processing, *Int. Mater. Rev.*, 2011, **56**, p 341-388.
- J. Vaithilingam, R.D. Goodridge, R.J.M. Hague, S.D.R. Christie, and S. Edmondson, The Effect of Laser Remelting on the Surface Chemistry of Ti6Al4V Components Fabricated by Selective Laser Melting, *J. Mater. Process. Technol.*, 2016, **232**, p 1-8.
- E. Chikarakara, S.N. Aqida, D. Brabazon, S. Naher, J.A. Picas, M.P. Fuste, and A. Forn, Surface Modification of HVOF Thermal Sprayed WC-CoCr Coatings by Laser Treatment, *Int. J. Mater. Form.*, 2010, **3**, p 801-804.
- B. Das, G. Muvvala, A. Nath, and P.P. Bandyopadhyay, Effect of Cooling Rate on Residual Stress and Mechanical Properties of Laser Remelted Ceramic Coating, *J. Eur. Ceram. Soc.*, 2018, **38**, p 3932-3944.
- Irfan, M. Hu, L. Meng, and C. Shi, Laser Re-melting of Modified Multimodal Cr3C2-NiCr Coatings by HVOF: Effect on the Microstructure and Anticorrosion Properties, *Rev. Adv. Mater. Sci.*, 2023, **62**, p 20230127.

32. K. Deenadayalan, V. Murali, A. Elayaperumal, A.S. Kumar, S. Arulvel, and M.S. Asl, Friction and Wear Properties of Short Time Heat-Treated and Laser Surface Re-melted NiCr-WC Composite Coatings at Various Dry Sliding Conditions, *J. Mater. Res. Technol.*, 2022, **17**, p 3080-3104.
33. J.M.S. de Sousa, R.G.N. Silva, A.de.S.P. Pereira, C. Amaral, and M. Pereira, Effect of Laser Remelting on Tribological Performance of Ni-Cr-B-Si Coatings Deposited by Laser Metal Deposition, *Soldag. e Insp.*, 2020, **25**, p 1-13.
34. G. Vinay, N.K. Singh, S.W. Khan, R. Kant, and H. Singh, XPS Insights for Optimization of Laser-Remelting as a Post-processing Technique for Coatings, *Surf. Interfaces*, 2024, **47**, p 0-4.
35. E. Olakanmi, Optimization of the Quality Characteristics of Laser-Assisted Cold-Sprayed (LACS) Aluminum Coatings with Taguchi Design of Experiments (DOE), *Mater. Manuf. Process.*, 2014, **31**, p 1-10.
36. R. Singh, M. Martin, and N. Dahotre, Influence of Laser Surface Modification on Corrosion Behavior of Stainless Steel 316L and Ti-6Al-4V in Simulated Biofluid, *Surf. Eng.*, 2005, **21**, p 297-306.
37. H. Chen and D. Kong, Effect of Laser Remelting Power on Immersion Corrosion of Amorphous Al-Ti-Ni Coatings, *Coatings*, 2018, **8**, p 46.
38. R.M. Miranda, J. Gandra, P. Vilaca, L. Quintino, and T. Santos, *Surface Modification by Solid State Processing*, Woodhead Publishing, Sawston, 2014, p 1-183
39. B. Das, A. Nath, and P.P. Bandyopadhyay, Scratch Resistance and Damage Mechanism of Laser Remelted Thermally Sprayed Ceramic Coating, *Surf. Coat. Technol.*, 2019, **364**, p 157-169.
40. H. Chen, C. Xu, Q. Zhou, I.M. Hutchings, P.H. Shipway, and J. Liu, Micro-scale Abrasive Wear Behaviour of HVOF Sprayed and Laser-Remelted Conventional and Nanostructured WC-Co Coatings, *Wear*, 2005, **258**, p 333-338.
41. B. Das, A. Nath, and P.P. Bandyopadhyay, Online Monitoring of Laser Remelting of Plasma Sprayed Coatings to Study the Effect of Cooling Rate on Residual Stress and Mechanical Properties, *Ceram. Int.*, 2018, **44**, p 7524-7534.
42. G. Prashar, H. Vasudev, and L. Thakur, Influence of Heat Treatment on Surface Properties of HVOF Deposited WC and Ni-Based Powder Coatings: A Review, *Surf. Topogr. Metrol. Prop.*, 2021, **9**, p 43002.
43. K. Chong, Y. Zou, D. Wu, Y. Tang, and Y. Zhang, Pulsed Laser Remelting Supersonic Plasma Sprayed Cr₃C₂-NiCr Coatings for Regulating Microstructure, Hardness and Corrosion Properties, *Surf. Coat. Technol.*, 2021, **418**, p 127258.
44. R. de Medeiros Castro et al., Laser Remelting of WC-CoCr Surface Coated by HVOF: Effect on the Tribological Properties and Energy Efficiency, *Surf. Coat. Technol.*, 2021, **427**, p 127841.
45. S. Karthikeyan, V. Balasubramanian, and R. Rajendran, Developing Empirical Relationships to Estimate Porosity and Microhardness of Plasma-Sprayed YSZ Coatings, *Ceram. Int.*, 2014, **40**, p 3171-3183.
46. D. Thirumalaikumarasamy, K. Shanmugam, and V. Balasubramanian, Influences of Atmospheric Plasma Spraying Parameters on the Porosity Level of Alumina Coating on AZ31B Magnesium Alloy Using Response Surface Methodology, *Prog. Nat. Sci. Mater. Int.*, 2012, **22**, p 468-479.
47. A. Bansal, J. Singh, and H. Singh, Slurry Erosion Behavior of HVOF-Sprayed WC-10Co-4Cr Coated SS 316 Steel with and Without PTFE Modification, *J. Therm. Spray Technol.*, 2019, **28**, p 1448-1465.
48. ASTM E1920, Standard Guide for Metallographic Preparation of Thermal Sprayed Coatings 1, *ASTM Int.*, 2016, **03**, p 1-5.
49. W. Conshohocken, Standard Test Method for Vickers Indentation Hardness of Advanced Ceramics, *TEST*, 2003 <https://doi.org/10.1520/C1327-08.2>
50. W.A. González-Hermosilla, D. Chicot, J. Lesage, J.G. La Barbera-Sosa, I.C. Gruescu, M.H. Staia, and E.S. Puchi-Cabrera, Effect of Substrate Roughness on the Fatigue Behavior of a SAE 1045 Steel Coated with a WC-10Co-4Cr Cermet, Deposited by HVOF Thermal Spray, *Mater. Sci. Eng. A*, 2010, **527**, p 6551-6561.
51. L. Chen, D. Yi, B. Wang, H. Liu, and C. Wu, Mechanism of the Early Stages of Oxidation of WC-Co Cemented Carbides, *Corros. Sci.*, 2016, **103**, p 75-87.
52. P.V. Krasovskii, O.S. Malinovskaya, A.V. Samokhin, Y.V. Blagoveshchenskiy, V.A. Kazakov, and A.A. Ashmarin, XPS Study of Surface Chemistry of Tungsten Carbides Nanopowders Produced Through DC Thermal Plasma/Hydrogen Annealing Process, *Appl. Surf. Sci.*, 2015, **339**, p 46-54.
53. A. Katrib, F. Hemming, P. Wehrer, L. Hilaire, and G. Maire, The Multi-surface Structure and Catalytic Properties of Partially Reduced WO₃, WO₂ and WC + O₂ or W + O₂ as Characterized by XPS, *J. Electron Spectrosc. Relat. Phenom.*, 1995, **76**, p 195-200.
54. O.Y. Khyzhun, XPS, XES and XAS Studies of the Electronic Structure of Tungsten Oxides, *J. Alloys Compd.*, 2000, **305**, p 1-6.
55. M. Nakazawa and H. Okamoto, XPS Study of WC Formation Process, *Appl. Surf. Sci.*, 1986, **27**, p 85-92.
56. J. Tian, Y. Xue, X. Yu, Y. Pei, H. Zhang, and J. Wang, Solvothermal Synthesis of NiWO₄ Nanostructure and Its Application as a Cathode Material for Asymmetric Supercapacitors, *RSC Adv.*, 2018, **8**, p 41740-41748.
57. S. Daemi, M. Moalem-Banhangi, S. Ghasemi, and A.A. Ashkarran, An Efficient Platform for the Electrooxidation of Formaldehyde Based on Amorphous NiWO₄ Nanoparticles Modified Electrode for Fuel Cells, *J. Electroanal. Chem.*, 2019, **848**, p 113270.
58. Z.L. Li, Q. Shan, Y.H. Jiang, R. Zhou, and Y.D. Sui, Effect of Co Addition on the Microstructure of Matrix in Tungsten Carbide Reinforced Surface Composite, *Appl. Mech. Mater.*, 2013, **376**, p 54-59.
59. E. Iguchi, H. Sugimoto, A. Tamenori, and H. Miyagi, Theoretical Estimation of Overlapping Repulsive Energies, Polarizabilities, and Lattice Energy in WO₃, *J. Solid State Chem.*, 1991, **91**, p 286-295.

Publisher's Note Springer Nature remains neutral with regard to jurisdictional claims in published maps and institutional affiliations.

Springer Nature or its licensor (e.g. a society or other partner) holds exclusive rights to this article under a publishing agreement with the author(s) or other rightsholder(s); author self-archiving of the accepted manuscript version of this article is solely governed by the terms of such publishing agreement and applicable law.